TISSUE ENGINEERING: Part A
Volume 20, Numbers 1 and 2, 2014
© Mary Ann Liebert, Inc.
DOI: 10.1089/ten.tea.2012.0613

Beyond Burst Pressure: Initial Evaluation of the Natural History of the Biaxial Mechanical Properties of Tissue-Engineered Vascular Grafts in the Venous Circulation Using a Murine Model

Yuji Naito, MD, PhD,[1,*] Yong-Ung Lee, PhD,[2,*,†] Tai Yi, MD,[1,†] Spencer N. Church, BS,[1] Daniel Solomon, MD,[1] Jay D. Humphrey, PhD,[1,2] Toshiharu Shin'oka, MD, PhD,[1,†] and Christopher K. Breuer, MD[1,†]

We previously developed and validated a murine model for investigating neotissue formation in tissue-engineered vascular grafts (TEVGs). Herein, we present the first longitudinal assessment of both the microstructural composition and the mechanical properties of a TEVG through the process of neovessel formation (total scaffold degradation). We show that when (poly)glycolic acid-based biodegradable scaffolds were used as inferior vena cava interposition grafts in mice, the evolving neovessel developed biaxial properties that approached those of the native vein within 24 weeks of implantation. Further, we found that these changes in biaxial properties related temporally to extracellular matrix production and remodeling, including deposition of collagen (types I and III), elastic fibers (elastin and fibrillin-1), and glycosaminoglycans in addition to changes in matrix metalloproteinase (MMP)-2 and -9 activity. Improving our understanding of the mechanobiological principles underlying vascular neotissue formation in TEVGs holds great promise for improving the design of TEVGs and enabling us to continue the translation of this technology from the bench to the clinic.

Introduction

We developed the first tissue-engineered vascular graft (TEVG) to be successfully used in humans.[1] In a clinical pilot study investigating the use of this TEVG in congenital heart surgery, we demonstrated the feasibility of using this technology to create vascular conduits for use as large diameter vascular grafts in high-flow, low-pressure systems such as the Fontan circulation.[2] Long-term follow-up of this cohort of 25 patients for a mean of 6.7 years revealed no graft-related deaths and no graft failures.[3] This study confirmed the utility of this TEVG in humans, making it the first man-made vascular graft with growth capacity. This study also demonstrated that stenosis was the primary graft-related complication, affecting between 15% and 30% of patients, and that other graft-related complications were not significant problems when the graft was used for this particular application.[3] The development of a man-made vascular graft with growth capacity promises to significantly advance the field of congenital heart surgery, where somatic overgrowth (outgrowing a graft) is a significant problem.[4] Unfortunately, the relatively high incidence of stenosis in the TEVG is a significant barrier preventing the widespread use of this technology in the clinic. To take advantage of the growth potential of the TEVG, we must overcome the problem of stenosis.

We developed the murine inferior vena cava (IVC) interposition vascular graft model to investigate cellular and molecular mechanisms underlying vascular neotissue formation in a high-flow, low-pressure circuit.[5–7] We demonstrated that this murine model recapitulates many aspects of vascular neotissue formation described in both our human cohort and in our previous large animal work, although changes occur over a shorter time course.[7,8] Using this model system, we have gained valuable insight into the process of neovessel formation—the transformation of a scaffold seeded with cells into a living vascular conduit that resembles a native blood vessel in both structure and function. We discovered that the vascular neotissue formation is driven by migration of the host endothelial cells and smooth muscle cells (SMCs) from the neighboring blood vessel wall through an immune-mediated process orchestrated by the seeded cells using a paracrine mechanism.[9,10] So far, our studies have focused mainly on the cellular processes involved in vascular neotissue formation, less on formation of the

[1]Interdepartmental Program in Vascular Biology and Therapeutics, Yale University School of Medicine, New Haven, Connecticut.
[2]Department of Biomedical Engineering, Yale University, New Haven, Connecticut.
*These authors contributed equally to this study.
[†]*Current affiliation:* Tissue Engineering Program and Surgical Research, Nationwide Children's Hospital, Columbus, Ohio.

extracellular matrix (ECM) and the associated biomechanical factors.[7–10]

There is a growing literature highlighting the importance of mechanobiological principles on vascular physiology and pathophysiology.[11–15] For example, compliance mismatch between a vascular graft and the native vessel into which it is implanted has been demonstrated to be a critical factor, leading at times to the formation of neointimal hyperplasia and stenosis.[16,17] The biomechanical properties of a TEVG are determined primarily by the sum of the mechanical properties of the scaffold and the biomechanical properties of the ECM. In the case of a biodegradable scaffold, this process is dynamic and changes as the scaffold degrades and neotissue forms. To date, biomechanical characterization of TEVGs has been largely limited to characterization of the burst pressure and suture retention strength of the TEVG scaffold.[18–20] These critical parameters must be evaluated to determine the clinical utility of any TEVG scaffold and we have previously measured these parameters for our scaffold.[6] Nevertheless, given our successful clinical experience using this TEVG in the Fontan circulation, which demonstrates the lack of aneurysmal dilation or rupture up to 10 years after implantation, it is time to take the next step and move beyond a basic mechanical characterization and into a more sophisticated analysis so that we can begin to understand better the complex, dynamic mechanobiological processes. The purpose of this study is to describe the evolving biomechanical properties of the TEVG from implantation of a tissue-engineered construct through scaffold degradation and neovessel formation. This is a first step in beginning to understand the mechanobiological principles that guide vascular neotissue formation. Our hope is that an increased understanding of these principles will lead to strategies that can be incorporated into the development of improved second-generation TEVGs rationally designed to inhibit the formation of TEVG stenosis.

Materials and Methods

Graft fabrication, implantation, and harvest

Tubular scaffolds (0.9 mm internal diameter, 0.3 mm thick, 3 mm in length) were constructed from a nonwoven (poly)-glycolic acid (PGA) felt (Concordia Fibers) and coated with a copolymer sealant solution of ε-caprolactone and L-lactide (P[CL/LA]) (Absorbable Polymers International) as described previously.[5,6]

All animal procedures were approved by the Yale University Institutional Animal Care and Use Committee. Scaffolds were implanted as IVC interposition grafts, between the left renal vein and iliac bifurcation, in 60 female CB-17 SCID/bg mice (Taconic Farms) at ~8 weeks of age. CB-17 SCID/bg mice were selected based on our experience that these mouse strains had the lowest rate of graft-related stenosis, hence allowing us first to focus on the evolving structure and properties of the nonstenotic wall. Implantation was accomplished using microsurgical techniques as described previously,[7] and graft patency was assessed *in vivo* using a high-frequency ultrasound biomicroscopy system (Vevo 770; Visualsonics) equipped with a RMV-704 transducer. Tissue-engineered neovessels were harvested at 2 ($n=12$), 6 ($n=12$), 12 ($n=12$), and 24 weeks ($n=12$) following implantation surgery; unoperated IVCs were used as controls ($n=12$). Freshly harvested specimens were used for either immunohistochemical or biochemical analysis ($n=7$ per endpoint) or mechanical testing and morphological characterization following testing ($n=5$ per endpoint).

Mechanical testing

Control IVCs and TEVGs, at each prescribed time point, were harvested beginning just below the renal bifurcation (with the grafts, including 1–2 mm of IVCs on each side). After measuring the length of the specimens before and after excision, and its separate segments when appropriate, it was transported to the laboratory in an ice-cold phosphate-buffered physiological solution (PBS). The specimens were then cannulated with size matching, custom drawn glass micropipettes and secured with 6-O suture and a small drop of glue on each end, then placed within a custom computer-controlled biaxial testing system designed specifically for testing murine vessels[21] (Fig. 1). In the case of the TEVGs, the adjacent IVC aided in the requisite cannulation. All vessels were stretched to their individual *in vivo* axial stretch (λ_z^{iv}), which is defined as the ratio of the axial length of the specimen (for controls) or central segment (for TEVGs) before and after excision, and allowed to equilibrate for 30 min under physiological pressure and flow in the PBS. Note that these specimen-specific extensions were accomplished by changing the overall axial length of the vessel under interactive computer control using two opposing microstepper motors. The associated axial force was measured on-line using a force transducer connected to the distal cannula (Fig. 1A).

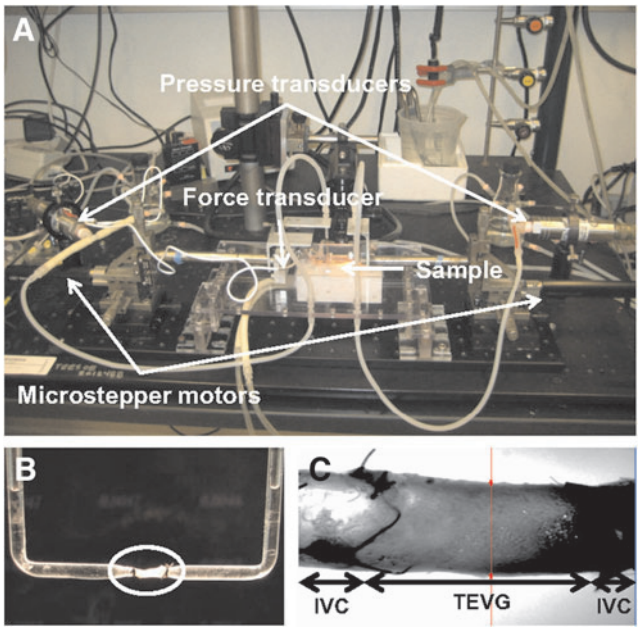

FIG. 1. **(A)** Photograph of the biaxial mechanical testing system; see Gleason *et al.*[21] for details. Resolution of the four primary measurements was 0.1 mmHg for pressure, 1.7 μm for diameter, 0.5 mN for axial force, and 0.2 μm for axial extension. **(B)** TEVG (in circle) mounted on a custom-made cannula for biaxial mechanical testing. **(C)** Representative specimen shown during biaxial mechanical testing; the TEVG is in the middle and the IVCs are on the left and right. TEVG, tissue-engineered vascular graft; IVC, inferior vena cava. Color images available online at www.liebertpub.com/tea

Mechanical testing was performed following the equilibration period plus four initial preconditioning cycles consisting of cyclic hydrostatic pressurization from 1 to 20 mmHg (i.e., physiological venous pressures) at λ_z^{iv}, with pressure monitored on-line using proximal and distal pressure transducers. Associated changes in the outer diameter were measured on-line using a side-mounted charge-coupled device camera and custom LabView software. Following preconditioning, unloaded dimensions (i.e., outer diameter and length) were remeasured within the device by interactively changing the length of the vessel until it began to bend at zero pressure. The native IVC or TEVG (central segment) was then returned to its *in vivo* axial stretch λ_z^{iv} and cyclic pressure-diameter data were collected over the range of 1–20 mmHg by means of a preprogrammed computer controlled protocol.

Finally, in addition to quantifying the pressure-diameter behavior, the so-called area compliance was computed at successive pressures using

$$C(P) = \frac{\Delta A(P)}{\Delta P}$$

where $\Delta A(P)$ is the change in the luminal area at a particular intraluminal pressure P. The luminal area was computed through the inner radius r_i, which in turn was inferred from on-line measurement of axial length and outer diameter by assuming incompressibility of the sample during pressurization. In particular, the inner radius r_i and wall thickness h were calculated using*

$$r_i - \sqrt{r_a^2 - \bar{V}/\pi l}$$
$$h = r_a - r_i$$

where $\bar{V}$ is the volume of the wall calculated in the unloaded state and l and r_a are the current length between the sutures and outer radius, respectively.

Histology and immunohistochemistry

Freshly explanted specimens were fixed overnight in a 4% paraformaldehyde phosphate-buffered saline solution, then embedded in paraffin as described previously.[7] For standard histology, sections were stained with hematoxylin and eosin, Masson's trichrome, Sirius red, Elastica van Gieson, or Hart's. For immunohistochemistry, sections were deparaffinized, rehydrated, and blocked for endogenous peroxidase activity and nonspecific staining. The primary antibodies used for staining included collagen I (Abcam), collagen III, fibrillin-1 (Abcam), matrix metalloproteinase (MMP)-2 (Millipore), and MMP-9 (R&D Systems). Antibody binding was detected using biotinylated secondary antibodies, followed by binding of streptavidin-HRP. Color development was performed by a chromogenic reaction with 3,3-diaminobenzidine (Vector). Nuclei were counterstained with hematoxylin; they were counted in five regions of each section and averaged for a total of four samples at each time point.

To estimate the volume of a polymer at each endpoint, histologic samples were observed under polarized light in which remnants of a scaffold were clearly demarcated by their birefringence. The remnant area was quantified using ImageJ (National Institute of Health). The volume was estimated based on the cross-sectional area and original length of the scaffold.

Biochemical analysis

An approximate 2-mm length of each fresh specimen was homogenized and lyophilized for quantitative biochemical analysis of collagen and elastin. In particular, the collagen content was determined by a Sircol™ colorimetric assay (Biocolor Assays, Inc.). Dry weights of lyophilized samples were measured, and samples were transferred to 1.5-mL microcentrifuge tubes containing 200 μL of pepsin (Sigma-Aldrich), with a concentration of 0.1 mg/mL of 0.5 M acetic acid to solubilize the collagen by means of overnight incubation. A standard curve was created using controls provided in the kit and the collagen content was inferred through spectrometry at 555 nm after precipitation and dye (Sirius red) binding to collagen. The elastin content was determined using a Fastin™ colorimetric assay (Biocolor Assays, Inc.). Dry weights of lyophilized samples were again measured and samples were transferred to 1.5-mL microcentrifuge tubes containing 100 μL of 0.25 M oxalic acid. The tubes were then placed on a heat block for 60 min at 100°C to convert insoluble elastin to water-soluble alpha-elastin. A standard curve was created using controls provided in the kit and the elastin content was detected through spectrometry at 513 nm after precipitation and dye binding of alpha-elastin.

RNA extraction, purification, and quantitative polymerase chain reaction

Freshly explanted specimens were frozen in optimal cutting temperature compund (OCT) (Tissue-Tek) and sectioned into forty 10-μm-thick sections using a Cryocut 1800 (Leica); excess OCT was removed by centrifugation in RNAse-free water. RNA was then extracted using the RNeasy Mini Kit (QIAGEN VWR) following the manufacturer's instructions. Reverse transcription was carried out with a 50 μL total volume containing 1 μg RNA, 5 μL 10×TaqMan RT Buffer, 11 μL magnesium chloride (25 mM), 10 μL dNTP mixture (10 mM), 2.5 μL Random Hexamer (50 mM), 1 μL RNase inhibitor (20 U/μL), and 1.25 μL reverse transcriptase (50 U/μL) (Applied Biosystems). RNAse-free water was added up to 50 μL. Thermal cycling parameters included incubation at 25°C for 10 min, reverse transcription at 48°C for 30 min, and inactivation at 95°C for 5 min.

Predesigned and validated gene-specific TaqMan Gene Expression Assays from Applied Biosystems were used in duplicate for quantitative real-time polymerase chain reaction (PCR) according to the manufacturer's instructions. Genes of interest included type I collagen (Col1a2, Mm00483888_m1), type III collagen (Col3a1, Mm01254458_g1), elastin (Eln, Mm00514692_m1), MMP-9 (Mmp9, Mm01240563_g1), and MMP-2 (Mmp2, Mm00439498_m1) (Applied Biosystems). Real-time PCRs were carried out in 96-well reaction plates in the CFX96 Touch™ Real-Time PCR Detection System (Bio-Rad) following the manufacturer's instructions. Relative expression levels were determined from collected data as threshold cycle numbers. Hypoxanthine-guanine phosphoribosyltransferase was used as an endogenous control.

Statistical analysis

All data are presented as mean ± standard error of the mean. Differences between groups were analyzed using

one-way analysis of variance followed by the Bonferroni's multiple comparison test. Statistical significance was considered as $p < 0.05$.

Results

All implanted grafts remained patent without stenosis or aneurysm formation and were harvested at one of the four predetermined endpoints: 2, 6, 12, or 24 weeks. Figure 2 shows representative photographs of TEVGs at each time of harvest (left panel) as well as representative ultrasound images (right panel) that reveal patency. Scaffolds were present in large amounts at 2 weeks, but completely degraded by 24 weeks, at which time they were replaced by neotissue. Histological evaluation over the implantation period revealed that the polymer had largely degraded by 6 weeks and was nearly absent at 12 weeks (Fig. 3A). Hence, the total volume of the scaffold, which was calculated from polarized light microscopic images, had decreased by half at 2 weeks and was nearly zero at 12 weeks (Fig. 3B). Overall, the TEVG wall thickness also decreased significantly from 2 to 6 weeks, but this thickness was essentially maintained up to 24 weeks (Fig. 3C). In particular, the TEVG wall thickness at 24 weeks was about 50% of the value at 2 weeks (149 ± 12.64 vs. $285 \pm 23.89\,\mu m$), which was nonetheless significantly greater than the native IVC ($21.98 \pm 0.8\,\mu m$).

Pressure-diameter data collected for the TEVG at its measured *in vivo* axial length (Fig. 4) revealed macroscopic

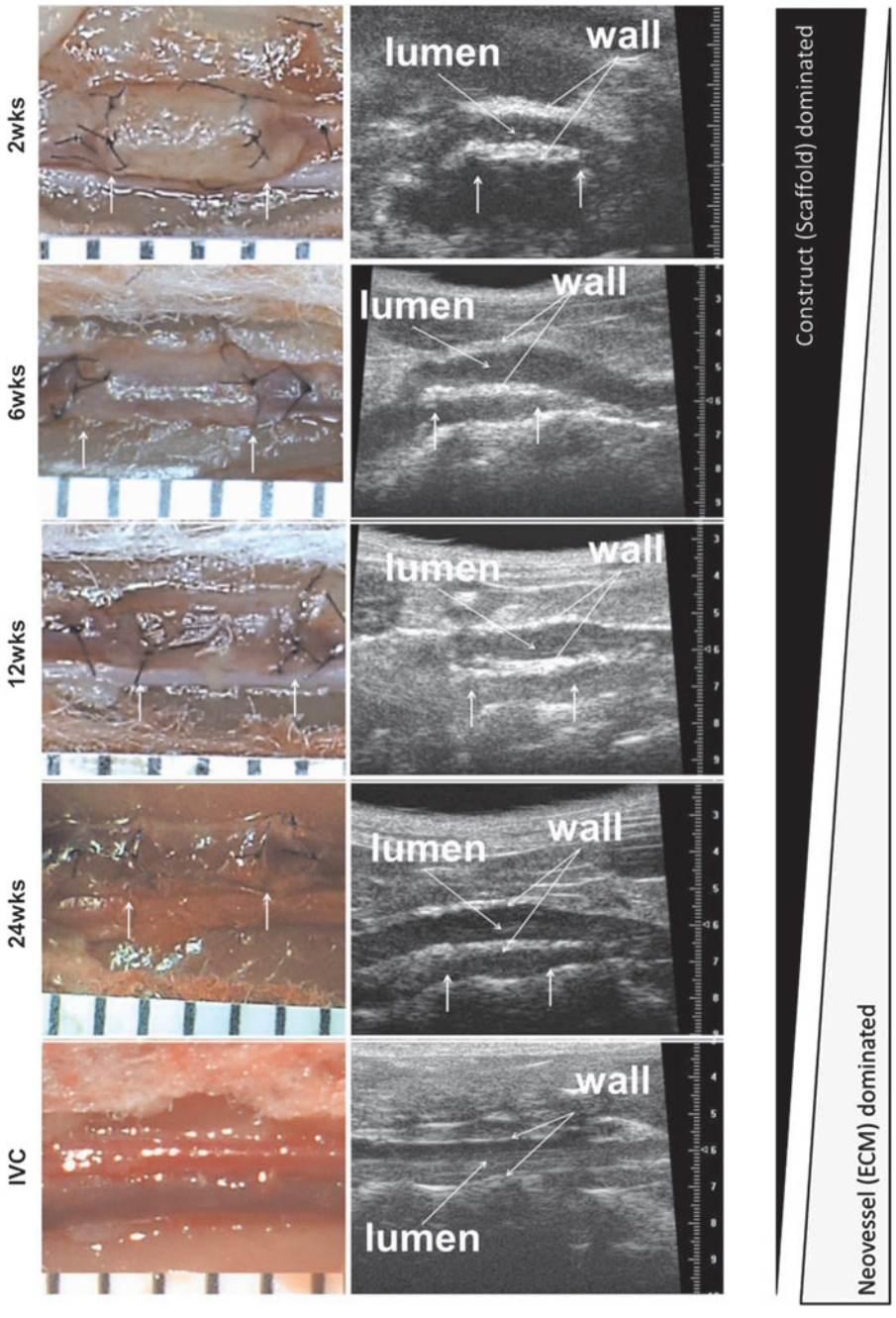

FIG. 2. Implanted TEVGs transformed into living blood vessels over a 24-week period. Arrows indicate the sites of anastomosis. The left panel shows gross images of TEVGs after implantation at each time point. At 2 weeks, the TEVG still showed a large amount of scaffold, which subsequently degraded and was completely replaced with neotissue at 24 weeks. Ultrasound images (right panel) show patency of the implanted TEVGs at each of the four time points. Color images available online at www.liebertpub.com/tea

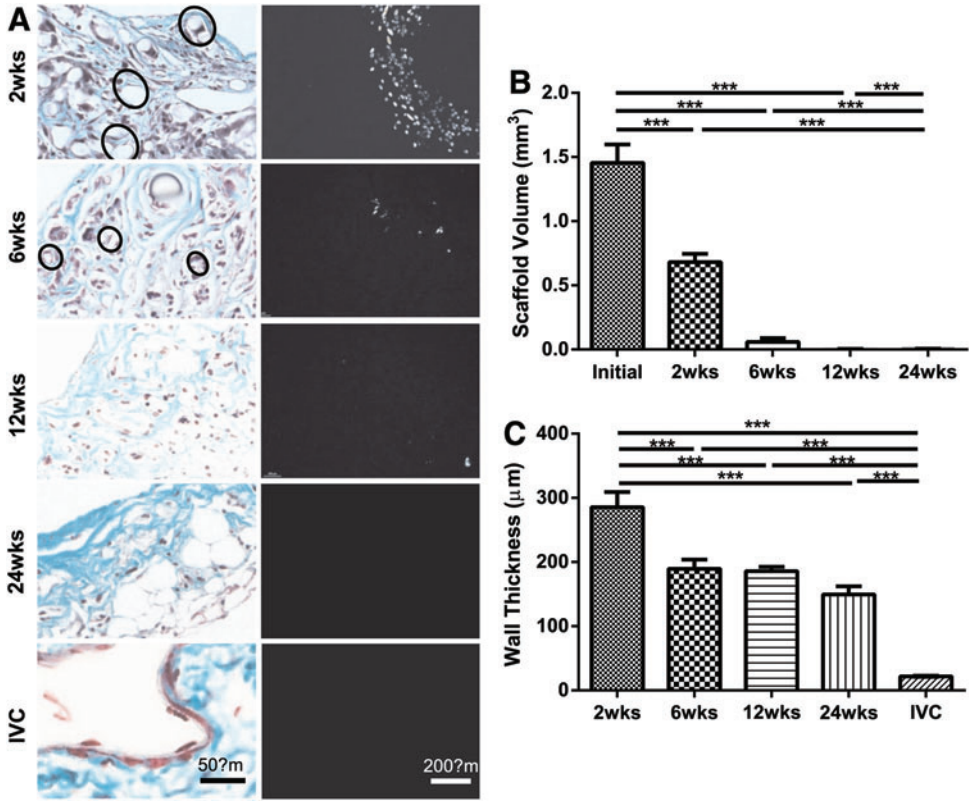

FIG. 3. Implanted scaffolds were completely degraded over 24 weeks and replaced with neotissue. Masson's trichrome staining **(A,** left panel**)** indicates remaining scaffold (marked with circles) at 2 and 6 weeks, but near complete loss by 12 weeks. The remaining scaffold volume was measured with polarized light images **(A,** right panel**)**. The scaffold volume **(B)** was decreased by half within 2 weeks, and nearly no scaffold was detected by 12 weeks. The wall thickness **(C)** decreased due to scaffold degradation, but the rate of overall decrease was much slower than scaffold degradation due to associated neotissue formation. Values are mean ± standard error of the mean (SEM) (***$p < 0.001$). Color images available online at www.liebertpub.com/tea

consequences of the formation of neotissue as the scaffold degraded over the 24-week period; there was a clear progression in mechanical behavior toward that of the native IVC. Overall, the TEVGs at 6 and 12 weeks showed an ~15% increase in diameter when pressurized from 1 to 20 mmHg, whereas the TEVGs at 24 weeks showed an ~31% increase in diameter when pressurized over the same range. For comparison, the native IVC showed an ~41% increase in diameter when pressurized from 1 to 20 mmHg. Values of the outer diameter at 20 mmHg for the 24-week TEVGs and IVCs, respectively, were significantly different than those for the 2-, 6-, and 12-week TEVGs ($p < 0.05$ for 24-week TEVG and $p < 0.001$ for the IVCs).

Figure 5 explicitly shows the evolution of the TEVG area compliance over the 24-week period of study as a function of luminal pressure, noting that IVC pressure is ≤5 mmHg *in vivo*. In particular, at 2 mmHg, the 24-week TEVGs were as compliant as the native IVCs (0.19 ± 0.03 vs. 0.22 ± 0.02 mm^2/mmHg) and thus significantly more compliant than TEVGs at 2, 6, and 12 weeks. Between 4 and 6 mmHg, the compliance of the 24-week TEVGs and IVCs were also significantly higher than that at 2 weeks, although not for 6 and 12 weeks.

In addition to the pressure-diameter data, measured changes in the *in vivo* axial stretch provided insight into the evolution of biaxial mechanical properties. Figure 6 shows measured *in vivo* axial stretches for TEVGs and adjacent IVCs. For TEVGs, the *in vivo* axial stretch was almost unity at 2 weeks, that is, there was essentially no retraction upon excision; however, this value increased significantly at 6 weeks (1.00 ± 0.01 vs. 1.21 ± 0.05, $p < 0.01$) and remained constant thereafter. In contrast, the initial *in vivo* axial stretch of the adjacent IVCs was near the native value of 1.44, but it decreased significantly at 6 weeks (1.44 ± 0.04 vs. 1.13 ± 0.03, $p < 0.01$), then gradually increased over the implantation period. These data thus suggest that the TEVG remodeled biaxially and that the adjacent IVC also remodeled in response to the

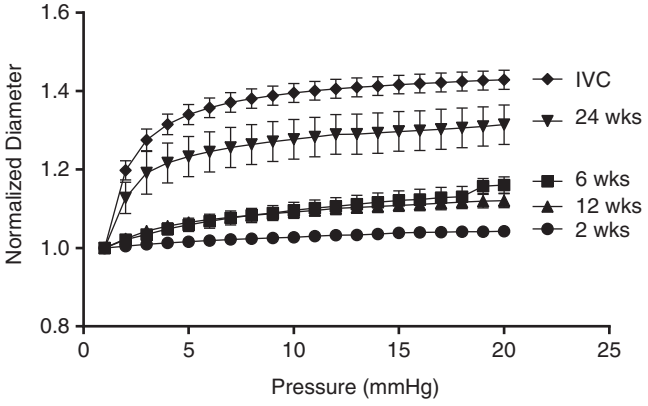

FIG. 4. *In vitro* pressure-diameter responses showed a gradual increase in distensibility over the implantation period and that the response of the TEVGs became similar to the native IVC by 24 weeks. Specifically, at 2 weeks, the TEVG showed almost no response to the increase in pressure; at 6 and 12 weeks, however, the TEVGs became more responsive to applied pressure and distended up to 10% at 20 mmHg. At 24 weeks, the TEVGs were more distensible and the shape of the curve became close to native IVC. This result clearly shows the transition from a stiff scaffold-dominated mechanical behavior to a more distensible, neotissue-dominated mechanical behavior. Values are mean ± SEM.

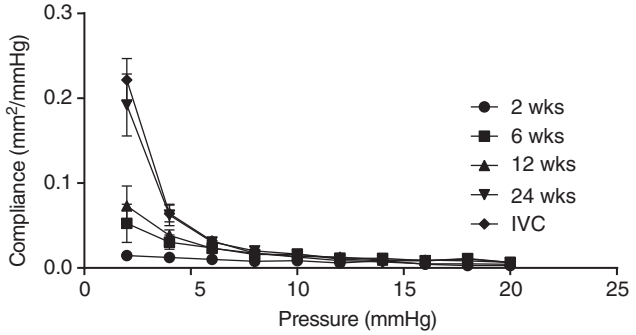

FIG. 5. Compliance of the TEVGs gradually increased and became similar to that of the native IVC. At 2 weeks, the TEVGs showed a very stiff behavior due to the scaffold-dominated mechanical properties; the compliance increased gradually by 6 and 12 weeks, however, due to degradation of the scaffold and formation of the less stiff neotissue. At 24 weeks, the compliance was similar to that of the native IVC. This result shows that not only does the neotissue replace the degrading scaffold, the behavior of the evolving neotissue also comes to resemble the native vessel. Values are mean ± SEM.

presence of the implanted graft. Understanding and optimizing graft–host interactions is likely critical to the overall long-term success of TEVGs.

Elastin was found, using Hart's staining, in the inner region of the neovessel at 6 weeks and thereafter, which was further corroborated by the Fastin assay (Fig. 7A, left panel; C). The qPCR results for tropoelastin (not shown) and fibrillin-1 (Fig. 7B) similarly revealed a significantly higher gene expression for fibrillin-1 at 2 weeks, followed by a marked decrease to a steady state level, as well as an increased gene expression for tropoelastin, particularly at 24 weeks. Hence, expression of fibrillin-1 appeared to precede the accumulation of elastin.

Immunohistochemistry revealed an early increase (i.e., at 2 weeks) in both type I and type III collagen, distributed diffusely with the scaffold (Fig. 7A, middle and right panel). The amounts of type I and III collagen tended to decrease thereafter, consistent with overall measurements using the Sircol assay (Fig. 7D). Note the gross similarity in collagen density between the TEVG at 24 weeks and the native IVC. Finally, note too that the qPCR results (not shown) also suggested an increased gene expression for types I and III collagen, particularly at 2 weeks.

Immunohistochemistry and MMP-2-positive cell counts both revealed that production and expression, respectively, of MMP-2 peaked at 6 weeks, but were similar at 2, 12, and 24 weeks (Fig. 8A, left panel; B). In contrast, results for MMP-9-positive cell counts revealed a dramatic peak at 2 weeks followed by a steady monotonic decrease toward values similar to those found in native IVC (Fig. 8A, right panel; C). MMP-9 is produced largely by macrophages; hence, its early appearance and subsequent rapid decrease may suggest an early, transient effect on remodeling due to macrophages. The delayed peak for MMP-2 may similarly be explained by its primary secretion by SMCs or myofibroblasts, which may have increased in number or synthetic activity later during the neovessel development.

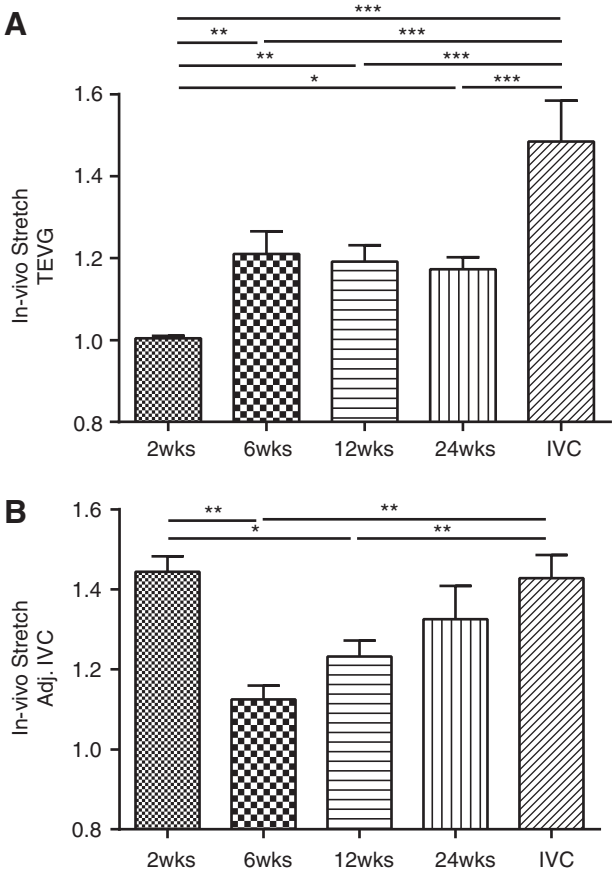

FIG. 6. Changes in the *in vivo* axial stretch show biaxial adaptation and remodeling of the TEVGs and adjacent IVCs. The TEVG's axial stretch **(A)** increased significantly from nearly 1 (i.e., no axial retraction upon excision) to near 1.2 (i.e., 20% retraction) by 6 weeks of implantation. In contrast, adjacent IVC's axial stretch **(B)** decreased from near native values of 1.4 to <1.2 at 6 weeks, but then gradually returned toward its native value over the implantation period. These results show that not only does the implanted graft undergo biomechanical remodeling and adaptation, the native vessels on both sides of the graft also undergo significant biomechanical adaptation due to the changes in the biomechanical environment as well. Values are mean ± SEM. $*p < 0.05$, $**p < 0.01$, $***p < 0.001$.

Discussion

To date, there has been limited information describing the mechanical properties of TEVGs beyond measurement of burst pressure or suture retention strength.[18–20,22] Given the growing body of literature supporting the central importance of mechanobiological responses in vascular biology and the development of vascular disease, we have begun to characterize the evolving biomechanical properties of TEVGs in the hope of identifying roles of mechanobiological processes in neovessel formation, which is complex and dynamic. In native blood vessels, vascular cells respond to changes in the biomechanical environment by remodeling their ECM to promote mechanical homeostasis.[14] Here, we hypothesize that a similar process—biomechanical and functional growth, remodeling, and adaptation—occurs during neovessel formation.

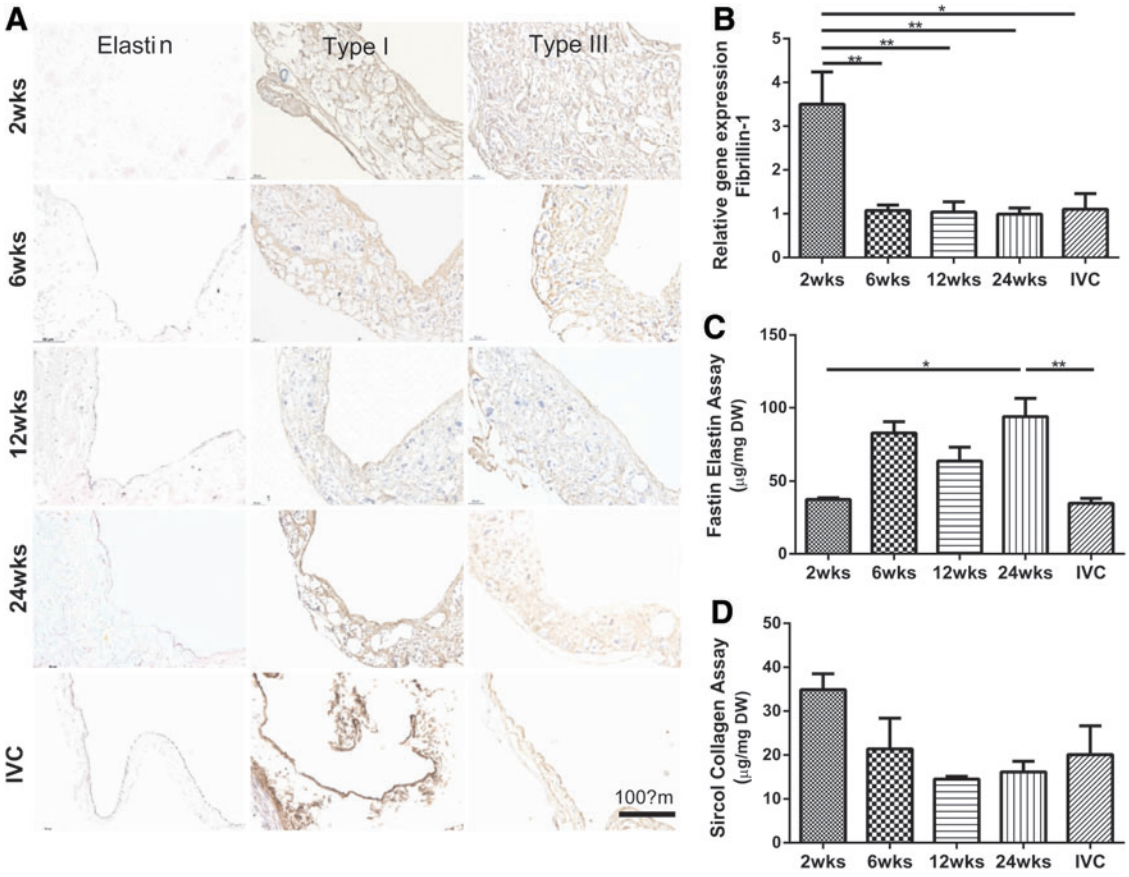

FIG. 7. Overall evolution of accumulated fibrillin-1 (an elastin-associated glycoprotein responsible for long-term structural stability), elastin, and collagen. Representative immunohistochemical results for elastin and fibrillar collagens (type I and III) within the TEVGs at each endpoint as well as the native IVC control **(A)**. Initially, relative gene expression of fibrillin-1 **(B)** increased significantly in comparison to that of native IVC, but decreased sharply and remained essentially unchanged after 6 weeks. Following an initial increase in fibrillin-1, the total amount of elastin **(C)** increased at 6 weeks and stayed elevated at 24 weeks. In contrast, there was an abrupt increase in collagen at 2 weeks **(D)**, followed by a decrease at 6 and 12 weeks, after which a steady state may have been reached. Values are mean ± SEM. $*p < 0.05$, $**p < 0.01$. Color images available online at www.liebertpub.com/tea

As a first step in investigating this process, we characterized evolving pressure-diameter responses and areal compliance of TEVGs over a long period (24 weeks) of neovessel formation. We previously showed that the associated scaffold, consisting of a PGA-based copolymer, largely degrades within 4 weeks of implantation and is replaced during this period primarily by fibrillar collagens (types I and III), with some type IV collagen, elastin, and glycosaminoglycans.[23] Yet, total polymer degradation requires ~26 weeks and there is continued neotissue formation and remodeling during this extended period. Earlier data collected at 1, 2, and 4 weeks revealed further that deposition of type III collagen preceded that of type I, not unlike in wound healing, and similarly that deposition of fibrillin-1 preceded that of elastin, not unlike that in development.[24] Proteoglycans were also deposited throughout the earlier 4-week study period, with versican preceding decorin. The former tends to associate with hyaluronan and is important during development in facilitating cell migration, whereas the latter is important during the assembly of collagen I into larger fibers.[25] Collectively, therefore, these findings are consistent with a sequential building of a neovessel having an evolving ECM composition, which reflects that seen during development.

Motivated by these previous findings, in this article, we presented novel longer term biological and biomechanical testing data collected over 24 weeks following implantation of IVC interposition TEVGs in the mouse. In particular, we quantified *in vitro* pressure-diameter responses of the TEVGs at their evolving *in vivo* axial stretches and found a progressive biaxial development and remodeling of neotissue that tended to yield a behavior similar to that of the native IVC by 24 weeks. When considered in combination with our earlier results,[23] early development of neotissue appears to parallel the rapid degradation of polymer (over the first 2 weeks) and to initiate in part because of a marked early increase in MMP-9 activity (presumably due to invading macrophages), followed by increased activity of MMP-2 at 6 weeks (presumably due to SMCs and myofibroblasts), as well as production of fibrillin-1, versican, and collagens III and I. As it can be seen in Figure 4, there was an associated decrease in stiffness (which is the inverse of compliance, cf. Fig. 5) and increase in distensibility over the first 6–12 weeks following implantation of the TEVG. Of particular interest, however, the pressure-diameter data also revealed a significant continued decrease in stiffness and increase in distensibility toward native behavior (Fig. 4, 24-week data) despite

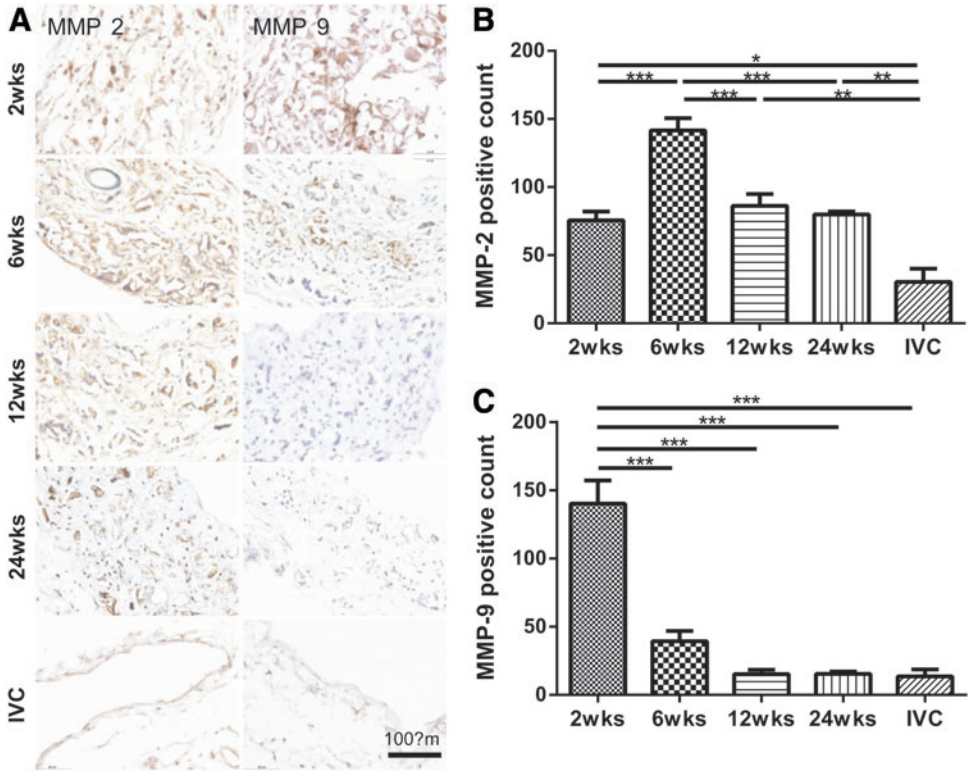

FIG. 8. MMP-2 and −9 increased initially, then decreased over time which represents early remodeling of the extracellular matrix. **(A)** Representative immunohistochemical results for MMP-2 and MMP-9 within the TEVGs at each endpoint as well as the native IVC control. MMP-2 activity **(B)** peaked at 6 weeks and gradually decreased at 24 weeks, but remained twofold higher than baseline. In contrast, MMP-9 activity **(C)** was elevated significantly at 2 weeks, but decreased monotonically thereafter toward a baseline value. Values are mean ± SEM. $*p < 0.05$, $**p < 0.01$, $***p < 0.001$. MMP. Color images available online at www.liebertpub.com/tea

an insignificant decrease in thickness from 12 to 24 weeks, and similarly, insignificant changes in the *in vivo* axial prestretch, elastin, collagen, and MMPs during this same period. This finding may suggest that an early production of the matrix, in response to the dramatic early changes in chemomechanical stimuli resulting from the degradation of polymers, may be followed by a more subtle, but equally important mechanobiological remodeling of the neotissue. Such a scenario would be consistent with the observed early production of versican and later production of decorin, the latter of which is important in fibrillogenesis and the building of larger collagen fibers.[25]

Whereas it is conventional to test only the vessel of interest, adjacent segments of the IVC were included to aid cannulation due to the short length of the TEVG (~3 mm long). The lower axial stiffness of the IVCs was accounted for naturally by performing pressure-diameter tests on the TEVGs at their individual *in vivo* axial stretches, based on interactive measurements of the length of the central segment. Because of continuity of axial force (i.e., the *in vivo* value), this also placed the adjacent segments of IVC at or near their individual *in vivo* axial stretches (i.e., at a higher stretch because of their lower axial stiffness). We did not collect pressure-diameter data on the adjacent segments of IVC, however. Despite the presence of continuity of axial force in these quasi-static tests, we also did not perform associated axial force-length tests on either the TEVG or the segments of IVC due in part to the need to track separately in real time, the associated axial stretches of the TEVG and IVC. Nevertheless, direct measurement of *in vivo* axial stretches for both segments provided an important insight into their axial adaptation and remodeling (cf. Fig. 6). Interestingly, there was a dramatic increase in λ_z^{iv} within the first 6 weeks for the TEVG, with no significant change thereafter (Fig. 6, top panel). Such increases tended to render the overall TEVG behavior biaxially closer to that of the native IVC, thus reminding us that biaxial mechanics must be considered as we continue to quantify and understand tissue-engineered vessels. An adaptive change in λ_z^{iv} is consistent with recent findings for native arteries wherein such changes appear to be among the first in many cases of vascular growth or remodeling.[26] Such behavior is understandable since circumferential and axial stiffness, and hence stresses, are coupled tightly, and changes in axial stretch can affect both axial and circumferential mechanics. Most of the earlier reports on native arteries show decreases in axial stretch, however, as an adaptive response to changes in hemodynamic loads. Indeed, the native IVCs experienced dramatic decreases in axial stretch at 2 weeks, although the stretches tended to return toward normal over the remainder of the study period. Taken together, these results remind us that not only do the implanted TEVGs undergo significant biomechanical remodeling, the adjacent native vessel experiences significant adaptation as well.

This study represents an important first step toward a detailed biomechanical quantification of the evolving macroscopic biomechanical properties and an associated characterization of microstructural changes within both the scaffold and the ECM of a TEVG through the process of neovessel formation. Much more remains to be accomplished, however. There is a need for more complete biaxial testing (e.g., multiple pressure-diameter and axial force-length protocols), assessments of possible evolving anisotropy and compressibility (through both three-dimentional imaging during testing and associated structural information from scanning electron or confocal microscopy, or both), and

formulation of an appropriate nonlinear constitutive relation for the evolving TEVG.[27] Indeed, there is also a need to delineate better the separate evolution of the TEVG and adaptation of the adjacent IVC (which will require tracking axial fiducial markers on each segment during biaxial testing). Finally, there is a need to elucidate the fundamental mechanobiological principles involved in neotissue formation in the hope of understanding their impact on vascular tissue regeneration and the development of graft-related complications such as the formation of TEVG stenosis. Not only would this improve our understanding of the mechanism of action of the TEVG, which would enable rational design over empiric experimentation, it would also enable computational modeling of this process, which could accelerate the development of improved second-generation TEVGs.

Acknowledgment

This research was supported, in part, by R01-HL098228 (C.B.).

Disclosure Statement

Dr. Breuer and Dr. Shin'oka received a grant support from Gunze Ltd. and Pall Corp. No corporate funding was used for this study.

References

1. Shin'oka, T., Imai, Y., and Ikada, Y. Transplantation of a tissue-engineered pulmonary artery. N Eng J Med **344,** 532, 2001.
2. Shin'oka, T., Matsumura, G., Hibino, N., Naito, Y., Watanabe, M., Konuma, T., Sakamoto, T., Nagatsu, M., and Kurosawa, H. Midterm clinical result of tissue-engineered vascular autografts seeded with autologous bone marrow cells. J Thorac Cardiovasc Surg **129,** 1330, 2005.
3. Hibino, N., McGillicuddy, E., Matsumura, G., Ichihara, Y., Naito, Y., Breuer, C., and Shinoka, T. Late-term results of tissue-engineered vascular grafts in humans. J Thorac Cardiovasc Surg **139,** 431, 2010.
4. Dearani, J.A., Danielson, G.K., Puga, F.J., Schaff, H.V., Warnes, C.W., Driscoll, D.J., Schleck, C.D., and Ilstrup, D.M. Late follow-up of 1095 patients undergoing operation for complex congenital heart disease utilizing pulmonary ventricle to pulmonary artery conduits. Ann Thorac Surg **75,** 399, 2003.
5. Nelson, G.N., Mirensky, T., Brennan, M.P., Roh, J.D., Yi, T., Wang, Y., and Breuer, C.K. Functional small-diameter human tissue–engineered arterial grafts in an immunodeficient mouse model: preliminary findings. Arch Surg **143,** 488, 2008.
6. Roh, J.D., Nelson, G.N., Brennan, M.P., Mirensky, T.L., Yi, T., Hazlett, T.F., Tellides, G., Sinusas, A.J., Pober, J.S., Saltzman, W.M., Kyriakides, T.R., and Breuer, C.K. Small-diameter biodegradable scaffolds for functional vascular tissue engineering in the mouse model. Biomaterials **29,** 1454, 2008.
7. Roh, J.D., Sawh-Martinez, R., Brennan, M.P., Jay, S.M., Devine, L., Rao, D.A., Yi, T., Mirensky, T.L., Nalbandian, A., Udelsman, B., Hibino, N., Shinoka, T., Saltzman, W.M., Snyder, E., Kyriakides, T.R., Pober, J.S., and Breuer, C.K. Tissue-engineered vascular grafts transform into mature blood vessels via an inflammation-mediated process of vascular remodeling. Proc Natl Acad Sci U S A **107,** 4669, 2010.
8. Mirensky, T.L., Nelson, G.N., Brennan, M.P., Roh, J.D., Hibino, N., Yi, T., Shinoka, T., and Breuer, C.K. Tissue-engineered arterial grafts: long-term results after implantation in a small animal model. J Pediatr Surg **44,** 1127, 2009.
9. Hibino, N., Villalona, G., Pietris, N., Duncan, D.R., Schoffner, A., Roh, J.D., Yi, T., Dobrucki, L.W., Mejias, D., Sawh-Martinez, R., Harrington, J.K., Sinusas, A., Krause, D.S., Kyriakides, T., Saltzman, W.M., Pober, J.S., Shin'oka, T., and Breuer, C.K. Tissue-engineered vascular grafts form neovessels that arise from regeneration of the adjacent blood vessel. FASEB J **25,** 2731, 2011.
10. Hibino, N., Yi, T., Duncan, D.R., Rathore, A., Dean, E., Naito, Y., Dardik, A., Kyriakides, T., Madri, J., Pober, J.S., Shinoka, T., and Breuer, C.K. A critical role for macrophages in neovessel formation and the development of stenosis in tissue-engineered vascular grafts. FASEB J **25,** 4253, 2011.
11. Ambrosi, D., Guillou, A., and Di Martino, E. Stress-modulated remodeling of a non-homogeneous body. Biomech Model Mechanobiol **7,** 63, 2008.
12. Cardamone, L., Valentín, A., Eberth, J.F., and Humphrey, J.D. Origin of axial prestretch and residual stress in arteries. Biomech Model Mechanobiol **8,** 431, 2009.
13. Gleason, R.L., Dye, W.W., Wilson, E., and Humphrey, J.D. Quantification of the mechanical behavior of carotid arteries from wild-type, dystrophin-deficient, and sarcoglycan-[delta] knockout mice. J Biomech **41,** 3213, 2008.
14. Humphrey, J.D. Vascular adaptation and mechanical homeostasis at tissue, cellular, and sub-cellular levels. Cell Biochem Biophys **50,** 53, 2008.
15. Humphrey, J.D., Eberth, J.F., Dye, W.W., and Gleason, R.L. Fundamental role of axial stress in compensatory adaptations by arteries. J Biomech **42,** 1, 2009.
16. Abbott, W.M., Megerman, J., Hasson, J.E., L'Italien, G., and Warnock, D.F. Effect of compliance mismatch on vascular graft patency. J Vasc Surg **5,** 376, 1987.
17. Lyman, D.J., Fazzio, F.J., Voorhees, H., Robinson, G., and Albo, D. Compliance as a factor effecting the patency of a copolyurethane vascular graft. J Biomed Mater Res **12,** 337, 1978.
18. L'Heureux, N., Dusserre, N., Konig, G., Victor, B., Keire, P., Wight, T.N., Chronos, N.A., Kyles, A.E., Gregory, C.R., Hoyt, G., Robbins, R.C., and McAllister, T.N. Human tissue-engineered blood vessels for adult arterial revascularization. Nat Med **12,** 361, 2006.
19. Hoenicka, M., Schrammel, S., Bursa, J., Huber, G., Bronger, H., Schmid, C., and Birnbaum, D.E. Development of endothelium-denuded human umbilical veins as living scaffolds for tissue-engineered small-calibre vascular grafts. J Tissue Eng Regen Med **7,** 324, 2013.
20. Ma, N., Wang, Z., Chen, H., Sun, Y., Hong, H., Sun, Q., Yin, M., and Liu, J. Development of the novel biotube inserting technique for acceleration of thick-walled autologous tissue-engineered vascular grafts fabrication. J Mater Sci: Mater Med **22,** 1037, 2011.
21. Gleason, R.L., Gray, S.P., Wilson, E., and Humphrey, J.D. A multiaxial computer-controlled organ culture and biomechanical device for mouse carotid arteries. J Biomech Eng **126,** 787, 2004.
22. L'heureux, N., Pâquet, S., Labbé, R., Germain, L., and Auger, F.A. A completely biological tissue-engineered human blood vessel. FASEB J **12,** 47, 1998.

23. Naito, Y., Williams-Fritze, M., Duncan, D.R., Church, S.N., Hibino, N., Madri, J.A., Humphrey, J.D., Shinoka, T., and Breuer, C.K. Characterization of the natural history of extracellular matrix production in tissue-engineered vascular grafts during neovessel formation. Cells Tissues Organs **195,** 60, 2012.
24. Wagenseil, J.E., and Mecham, R.P. Vascular extracellular matrix and arterial mechanics. Physiol Rev **89,** 957, 2009.
25. Wight, T.N. Arterial remodeling in vascular disease: a key role for hyaluronan and versican. Front Biosci **13,** 4933, 2008.
26. Niklason, L.E., Yeh, A.T., Calle, E.A., Bai, Y., Valentín, A., and Humphrey, J.D. Enabling tools for engineering collagenous tissues integrating bioreactors, intravital imaging, and biomechanical modeling. Proc Natl Acad Sci U S A **107,** 3335, 2010.
27. Ferruzzi, J., Bersi, M.R., and Humphrey, J.D. Biomechanical phenotyping of central arteries in health and disease: advantages of and methods for murine models. Ann Biomed Eng **41,** 1311, 2013.

Address correspondence to:
Christopher K. Breuer, MD
Research Institute Nationwide Children's Hospital
700 Children's Drive—WB4151
Columbus, OH 43205-2664

E-mail: Christopher.Breuer@nationwidechildrens.org

Received: October 12, 2012
Accepted: August 7, 2013
Online Publication Date: November 13, 2013